Chaos, Solitons & Fractals Vol. 2, No. 3, pp.281–301, 1992
Printed in Great Britain

0960-0779/92$5.00 + .00

Universality and Scaling in Two-Dimensional Coupled Map Lattices

S. P. KUZNETSOV

Institute of Radio Engineering and Electronics, Russian Academy of Sciences, Saratov, Russia

Abstract—The dynamics of two-dimensional coupled logistic map lattices near the onset of chaos is investigated using the concepts of renormalization group, universality and scaling. Two versions of RG approach and formulation of scaling properties are considered. The first one deals with lattice effects and the second one describes continuous limit behaviour. The examples of spatial patterns and spectra demonstrating both types of scaling are discussed.

INTRODUCTION

Coupled map lattices (CML) were introduced by several authors as simple models describing many peculiarities of the complicated dynamics of spatially extended systems (see, for example [1–12]). The most popular class of these models includes the lattices constructed by cells demonstrating a period doubling transition to chaos when some control parameter is varied. This kind of local dynamics is characterized by universality and scaling being explained with the help of the renormalization group (RG) approach by Feigenbaum [13, 14]. Due to the existence of universality and scaling for individual cells, one may also expect the appearance of some analogous properties for spatially extended lattices.

Various aspects of this idea were discussed earlier by Kuznetsov [4, 6], Kuznetsov and Pikovsky [5], Aranson *et al.* [8] and Kook *et al.* [12] for one-dimensional CMLs. It is evident that increasing the spatial dimension of the lattices is a natural and necessary step for the construction of more realistic models of turbulent states. The computer investigations of two-dimensional CMLs were undertaken by Kapral [3], Oppo and Kapral [7], Bohr and Christensen [9] and Kaneko [10, 11]. They discussed in detail diverse phenomena of two-dimensional pattern dynamics, but did not develop the renormalization group approach. Nevertheless, this method seems to be necessary for the understanding, classification and systematization of the phenomena observed in CML dynamics. Particularly, it gives an explanation of scaling property dependence on the form of coupling terms. This paper is devoted just to the investigation of the two-dimensional CML near the onset of chaos in the light of RG, universality and scaling concepts.

In general, the content of the RG approach is as follows: beginning with the evolution operator of the system for one time step we then construct the evolution operator over two steps. Performing some variable changes, we attempt to make the new operator as similar as possible to the old one. This procedure of RG transformation may be repeated many times giving the sequence of evolution operators over increasing temporal intervals of 4, 8, $\ldots 2^n \ldots$ steps. It may occur that there exists some critical point, line or surface in the system parameter space where the above operator sequence converges to a regular limit operator, this being the fixed point of the RG transformation. This operator must be universal because it is defined by properties of the RG transformation rather than by the

concrete initial evolution operator. Furthermore, the scaling properties of the parameter space structure near the critical situation are determined by the eigenvalue spectrum of the RG transformation linearized near the fixed point operator. Each essential eigenvalue with modulus larger than unity is responsible for the appearance of one essential parameter of the system. This eigenvalue gives a scaling constant for some direction in the parameter space. The number of such eigenvalues defines *the codimension* of the critical situation. This is just a number of parameters in a family of systems permitting this critical behaviour to be typical.

Two versions of RG approach will be proposed.

The first version deals with lattice effects. In this case, the evolution operator of an uncoupled map lattice at the onset of chaos is examined as the fixed point of the RG transformation. The second variant of RG approach works in the situation when the characteristic scale of spatial patterns is much larger than the lattice step. The procedure of RG transformation is accompanied now by rescaling the spatial variables by $\sqrt{2}$. The fixed point operator relates to a medium obtained in the continuous limit from the lattice with particular, dissipative type of coupling. The computer results are presented illustrating two types of scaling corresponding to both versions of the RG approach.

LATTICE RENORMALIZATION GROUP ANALYSIS

We begin by considering a two-dimensional square lattice of uncoupled identical cells governed by the evolution operator F

$$F\colon \{\ldots, x(i, j), \ldots\} \to \{\ldots, f(x(i, j)), \ldots\}, \tag{1}$$

where i, j are the spatial indices of the cells. We assume that the local map f belongs to Feigenbaum's universality class and demonstrates period-doubling transition to chaos under the increasing control parameter λ. The accumulation point of period-doubling bifurcations will be denoted by λ_c (the *critical* value).

Let us define the RG transformation R as a simultaneous application of Feigenbaum's doubling procedure [13, 14] to all maps forming the lattice:

$$R\colon \{\ldots, f(x(i, j)), \ldots\} \to \{\ldots, af(f(a^{-1}x(i, j))), \ldots\}, \tag{2}$$

where $a = -2.5029\ldots$ is the known universal scaling constant. While we consider the uncoupled lattice, the multiple repetition of procedure R at the critical point λ_c will give us the operator sequence $F_n = R^n F$ converging to the fixed point of the RG transformation R. This is the limit operator

$$G_L\colon \{\ldots, x(i, j), \ldots\} \to \{\ldots, g(x(i, j)), \ldots\}, \tag{3}$$

Here, g is Feigenbaum's universal function obeying the functional equation $g(x) = ag(g(x/a))$.

Now consider a small perturbation of the fixed point G_L maintaining the translation lattice invariance and including the coupling between the nearest-neighbour cells. For the weak coupling, the contribution of all the neighbours may be introduced into the dynamical equation additively. So, we have

$$\begin{aligned} F = G_L + \varepsilon H\colon \{\ldots, x(i, j), \ldots\} \to \{\ldots, g(x(i, j)) \\ +\varepsilon[h(x(i, j)) + \phi(x(i, j), x(i-1, j)) + \phi(x(i, j), x(i+1, j)) \\ +\phi(x(i, j), x(i, j-1)) + \phi(x(i, j), x(i, j+1)), \ldots\}, \end{aligned} \tag{4}$$

where h is the perturbation of individual cells while the ϕ terms introduce the coupling. Without losing generality, one may consider only the coupling functions $\phi(x, y)$ satisfying the condition $\phi(x, x) \equiv 0$. Let us perform the RG transformation (2) with a linear approximation in ε. The result may be written in the form of equation (4) again, but with new functions $h = \hat{M}h$ and $\phi = \hat{m}\phi$. The linear operators $\hat{M}$ and $\hat{m}$ are defined by the relations

$$\begin{aligned} \hat{M}&: h(x) \to a[g'(g(x/a))h(x/a) + h(g(x/a))], \\ \hat{m}&: \phi(x, y) \to a[g'(g(x/a))\phi(x/a, y/a) + \phi(g(x/a), g(y/a))], \end{aligned} \tag{5}$$

and coincide with those introduced by Feigenbaum [13, 14] and Kuznetsov [15], respectively. The essential eigenvalues whose moduli exceed one and which are not connected with infinitesimal variable changes are $\nu_0 = \delta = 4.669201\ldots$ for $\hat{M}$ and $\nu_1 = a = -2.5029\ldots$, $\nu_2 = 2$ for $\hat{m}$. The corresponding eigenfunctions are $h_0(x)$, see Ref. [14], and

$$\phi_1(x, y) = (x - y) + o(x, y) \text{ and } \phi_2(x, y) = (x^2 - y^2) + o(x^2, y^2), \tag{6}$$

see Refs [8, 15, 12].

The operator F_n, giving the evolution of the system over 2^n iterations of the initial map, may be written as a linear approximation near the fixed point G_L as

$$F_n: \{\ldots, x(i, j), \ldots\} \to \{\ldots, y(i, j), \ldots\}, \tag{7}$$

where

$$\begin{aligned} y(i, j) &= g(x(i, j)) + \Lambda\delta^n h(x(i, j)) \\ &\quad + C_1 a^n[\phi_1(x(i, j), x(i-1, j)) + \phi_1(x(i, j), x(i+1, j)) \\ &\quad + \phi_1(x(i, j), x(i, j-1)) + \phi_1(x(i, j), x(i, j+1))] \\ &\quad + C_2 2^n[\phi_2(x(i, j), x(i-1, j)) + \phi_2(x(i, j), x(i+1, j)) \\ &\quad + \phi_2(x(i, j), x(i, j-1)) + \phi_2(x(i, j), x(i, j+1))]. \end{aligned} \tag{8}$$

The perturbation with eigenvalue ν_0 is controlled by the λ parameter in the initial map, Λ being proportional to $\lambda - \lambda_c$. The perturbations with eigenvalues ν_1 and ν_2 correspond to the inclusion of two types of coupling, which have different properties with respect to the RG transformation. The first of them is called *inertial coupling* and the second—*dissipative coupling* or *diffusion*. They are characterized by the parameters C_1 and C_2, depending on the initial coupling function $\phi(x, y)$.

It follows from equation (8) that the regimes with similar spatio-temporal dynamics exist in the points of the parameter space (Λ, C_1, C_2) and $(\Lambda/\delta, C_1/a, C_2/2)$. The dynamical variable scale decreases by a and the temporal scale increases by two in the second point. We call it *the lattice scaling*.

What is the situation when the number of interacting neighbours increases? All the essential neighbours may be distributed over some number N of equivalence classes in respect of the symmetry group transformation of the lattice with fixed cell (i, j). Two parameters, for inertial and dissipative coupling, must be given for each equivalence class. So, the total number of essential parameters is $2N + 1$. The rescaling of parameters is accompanied now by changing all inertial coupling constants by a, dissipative coupling constants by two and difference $\lambda - \lambda_c$ by δ. This is true for any lattice configuration (rectangular, triangular, hexagonal).

COMPUTER SIMULATION AND LATTICE SCALING

Let us consider now, what conclusions may be drawn concerning the behaviour of two-dimensional lattices near the onset of chaos. The following methodology is used: at the beginning, one must choose the models suitable for computer investigation. Then, some initial results of numerical simulation must be obtained. It gives the preliminary rough understanding of the pattern dynamics in different regions of the parameter space. Such studies were performed by Kapral [3], Oppo and Kapral [7] and Kaneko [10, 11] for different coupling functions. Taking into account the above formulated scaling property, we state the possibility of realizing the whole hierarchy of similar dynamical states with greater temporal scales near the critical point of zero coupling. Thus, a fine structure of the parameter space in the vicinity of this point is revealed. Further, this hierarchy of states may be reproduced by special computer calculations. One may check the similarity of corresponding regimes using spatial diagrams, spectra and Lyapunov exponents.

We shall consider only the square lattices with nearest-neighbour coupling and use the logistic map $f(x) = 1 - \lambda x^2$ as an individual cell. It is known as the simplest representative of Feigenbaum's universality class. Taking into account the form of the eigenfunctions (6), one concludes that in the linearly coupled lattice [3, 7]

$$x_{n+1}(i, j) = f(x_n(i, j)) + (\varepsilon/4)[x_n(i+1, j) + x_n(i-1, j) + x_n(i, j+1) + x_n(i, j-1) - 4x_n(i, j)], \tag{9}$$

both types of coupling are present, with the inertial one dominating. On the contrary, the quadratic coupling [9–11]

$$x_{n+1}(i, j) = f(x_n(i, j)) + (\varepsilon/4)[f(x_n(i+1, j)) + f(x_n(i-1, j)) + f(x_n(i, j+1)) + f(x_n(i, j-1)) - 4f(x_n(i, j))], \tag{10}$$

is purely dissipative.

It is easy to see that the coupling in equation (10) is produced by averaging over neighbours, therefore its action tends to equalize their instantaneous states. It provides the ground for the term 'dissipative coupling'. On the other hand, equation (9) maintains the memory of the previous states when the state passes near the origin (in the order $\propto x$). It justifies the term 'inertial coupling'.

Using a combination of the coupling terms from equations (9) and (10), one can obtain the lattice with arbitrary 'composition' of coupling. So, the system with three parameters

$$x_{n+1}(i, j) = f(x_n(i, j)) + (\varepsilon_1/4)[x_n(i+1, j) + x_n(i-1, j) + x_n(i, j+1) + x_n(i, j-1) - 4x_n(i, j)] + (\varepsilon_2/4)[f(x_n(i+1, j)) + f(x_n(i-1, j)) + f(x_n(i, j+1)) + f(x_n(i, j-1)) - 4f(x_n(i, j))], \tag{11}$$

may be considered as a *universal model*. This is the simplest representative of the universality class connected with the RG fixed point G_L (for the case of square nearest-neighbour coupled lattices). It contains the full variety of phenomena intrinsic to this universality class in the arbitrary small vicinity of the critical point $\{\lambda = \lambda_c,\ \varepsilon_1 = 0,\ \varepsilon_2 = 0\}$.

It may be shown (see Appendix) that the parameters of inertial and dissipative coupling of equations (7) and (8) are connected with ε_1, ε_2 by the relations

$$C_1 = \varepsilon_1,\ C_2 = \varepsilon_2 - 0.088\,\varepsilon_1. \tag{12}$$

We begin with the case of purely dissipative coupling [see equation (10)] using the boundary conditions of periodicity

$$x(i + M, j) = x(i, j), x(i, j + M) = x(i, j). \tag{13}$$

Having taken the random initial conditions with uniform distribution on (0, 1) one finds the following basic phenomena classified by Kaneko [10, 11].

For small coupling ($\varepsilon \simeq 0.1$) and λ near the critical value, a *frozen random pattern phase* is observed. The domain structure is formed here; each domain is a set of adjacent cells oscillating in phase. The temporal dynamics inside the domains depends on their configurations and sizes and may become chaotic for supercritical λ. By increasing λ, the *pattern selection phase* arises leading to the formation of islands of *checkerboard patterns* demarcated by *chaotic strings* of complex, sinuous form. The temporal chaos is dumped in checkerboard pattern regions while the strings demonstrate slow random walks (*Brownian motion of chaotic strings*). The closed strings may collapse and die. After some long period of time all strings die if the lattice has an even size M. The further increase of λ provides the *phase of defect turbulence*, when the closed strings can not only die but also appear. At last, for larger λ, the *fully developed turbulence* arises when no long-living structures are present.

For larger coupling ($\varepsilon \simeq 0.2$) the same Kaneko phases are observed but the phase of pattern selection is characterized by the appearence of 2×1-type structures (with in-phase oscillation of two neighbour cells) rather than checkerboard patterns. For $\varepsilon \simeq 0.4$ the phase of frozen patterns does not take place: the temporal evolution is accompanied by the gradual squeezing and disappearance of the initially existing domains. The final state is spatially uniform in the subcritical range of λ and turbulent without long-living structures in the supercritical one.

According to the lattice scaling, all the named phenomena may be reproduced by increasing the temporal scale by 2^K if we reduce the $\lambda - \lambda_c$ value by δ^K, the coupling parameter ε by 2^K and the random initial condition amplitude by a^K. We call the number K the *scaling level*.

Let us consider the examples of similar Kaneko phases for different scaling levels. At the level $K = 0$ we take $\lambda = 1.54$, a random initial condition amplitude of 0.4 and two values of coupling parameter $\varepsilon = 0.1$ and $\varepsilon = 0.3$. For the following levels the rescaling is performed by the above rules.

Figures 1 and 2 show the snapshot patterns for the lattice of size 32×32. On lattice points (i, j), squares with lengths proportional to $a^K x(i, j)$ are depicted for the scaling level K. In Fig. 1 one can see the phases of Brownian motion of chaotic strings and in Fig. 2 the phases of fully developed turbulence. The visual consideration of the pictures supports the similarity of the spatio-temporal dynamics. For a more convincing verification we must calculate quantitative characteristics of the dynamics.

In Table 1 we present the values of maximal Lyapunov exponent L just for the cases shown in Fig. 2. Under transition from one scaling level to another, the values of L must be proportional to 2^{-K} because the characteristic temporal scale increases as 2^K. From the table one can see that the $L \cdot 2^K$ values coincide within the accuracy of the data. So, the scaling really takes place.

Figure 3 shows the spatial spectra for the same regimes but in the lattice 64×64. After a sufficiently large number of initial iterations to exclude transients, the averaging over several decades of temporal steps was performed for spatial Fourier amplitude squares of $x(i, j)$. The scaling property appears as a reproduction of the spectra shapes for different K levels, with a constant shift along the vertical axis in the semilog plot.

The case of linear coupling between the lattice cells was studied by Kapral [3] and Oppo

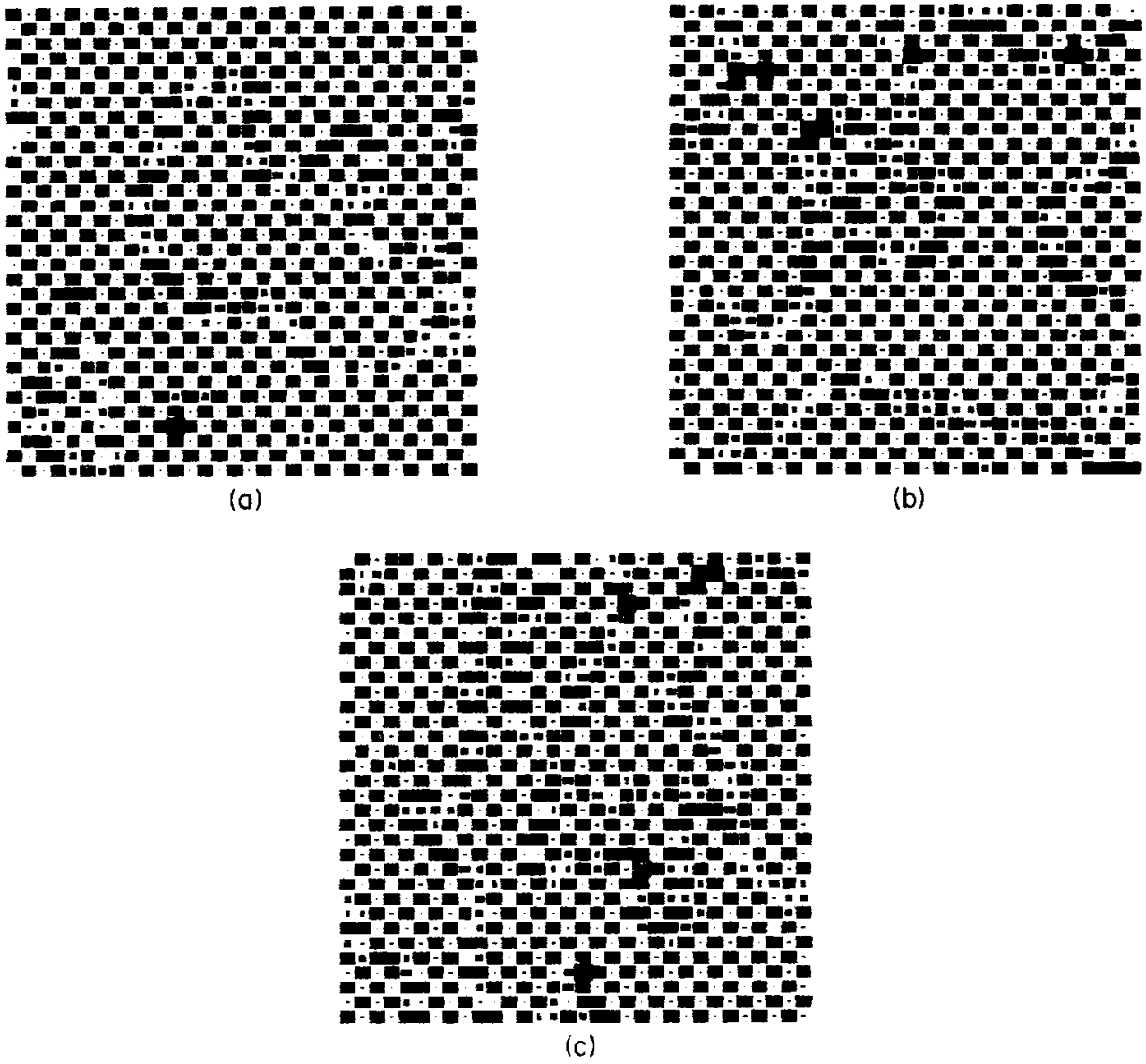

Fig. 1. Phase of chaotic string Brownian motion in the lattice with dissipative coupling (10) at three levels of lattice scaling K. The lattice size is 32×32 with periodic boundary conditions. The values $x(i, j)$ are coded by squares of size $\propto a^K x(i, j)$; (a) $K = 0$, $\lambda = 1.54$, $\varepsilon = 0.1$, the random initial condition amplitude $\Delta x_{\text{rnd}} = 0.4$, the iteration number $n = 400$, (b) $K = 1$, $\lambda = 1.430892$, $\varepsilon = 0.05$, $\Delta x_{\text{rnd}} = 0.16$, $n = 800$, (c) $K = 2$, $\lambda = 1.407524$, $\varepsilon = 0.025$, $\Delta x_{\text{rnd}} = 0.064$, $n = 1600$.

and Kapral [7]. One of the equations considered was just equation (9) within the trivial variable change. It was found that the phenomenon of forming checkerboard patterns is very typical. Such patterns may already arise in some parameter regions for subcritical λ. Depending on initial conditions, the domains of checkerboard patterns are formed being demarcated by string defects. The quasiperiodic temporal dynamics may be observed on the checkerboard pattern background with following transition to chaos under increasing λ. Also the cases of linear coupling with larger numbers of neighbours were considered. It was found that other structures begin to play the dominating role rather than the checkerboard ones. For example, the parallel strips with the wavelength of two dominate in the nine-neighbour lattice and those with the wavelength of four in the thirteen-neighbour one.

As we have already noticed, the linear coupling is a combination of inertial and dissipative types, and the first one dominates. Under multiple RG transformations the

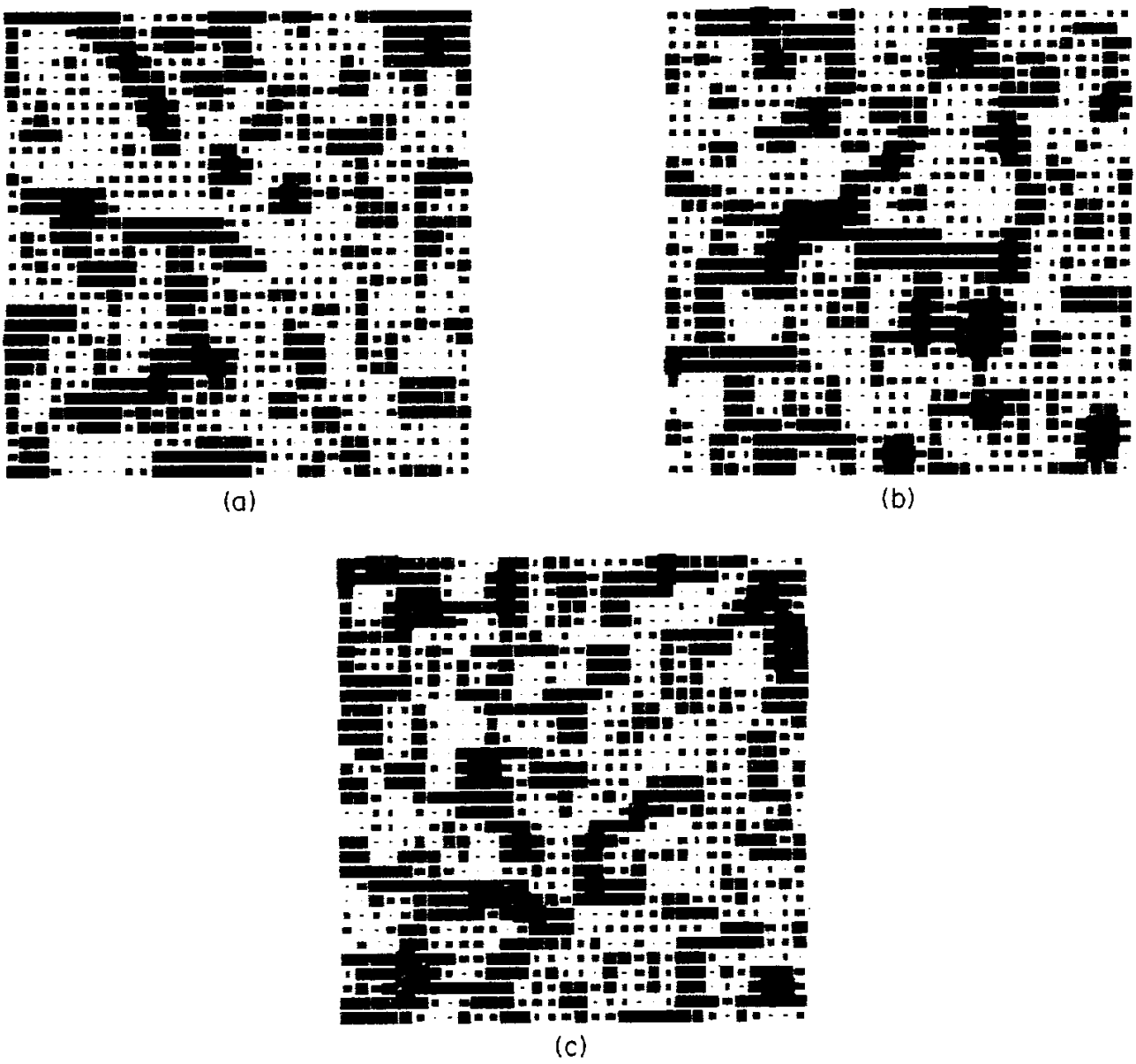

Fig. 2. Developed turbulence phase in the lattice with dissipative coupling (10) at three levels of lattice scaling. The coupling parameter values (a) $\varepsilon = 0.3$, (b) $\varepsilon = 0.15$, (c) $\varepsilon = 0.075$. Other parameters and visualization rules are the same as in Fig. 1.

Table 1. The maximal Lyapunov exponent L for states of the model (11) similar in the sense of the lattice scaling. The type of coupling: pure dissipative (upper block), pure inertial (middle block), composite (lower block). The lattice size is 32×32 with periodic boundary conditions and random initial conditions with amplitude Δx_{rnd}

K	λ	ε_1	ε_2	Δx_{rnd}	L	$L \cdot 2^K$
0	1.540000	0	0.3	0.4	0.144 ± 0.008	0.144 ± 0.008
1	1.430892	0	0.15	0.16	0.071 ± 0.004	0.142 ± 0.008
2	1.407524	0	0.075	0.064	0.035 ± 0.002	0.140 ± 0.008
0	1.540000	0.1	0.0088	0.4	0.403 ± 0.008	0.403 ± 0.008
1	1.430892	−0.03995	−0.00352	0.16	0.206 ± 0.004	0.411 ± 0.008
2	1.407524	0.01596	0.00140	0.064	0.102 ± 0.002	0.409 ± 0.008
0	1.540000	0.36	0.3	0.4	0.118 ± 0.008	0.118 ± 0.008
1	1.430892	−0.14383	0.12150	0.16	0.061 ± 0.004	0.122 ± 0.008
2	1.407524	0.05747	0.07214	0.064	0.030 ± 0.002	0.121 ± 0.008

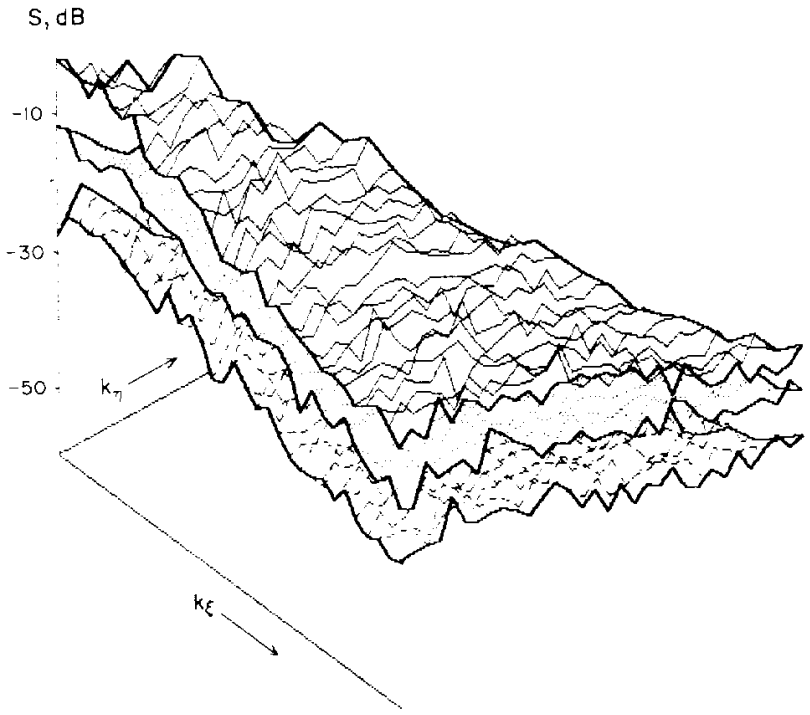

Fig. 3. Spatial spectra for three turbulent states similar in the sense of the lattice scaling: logarithm of temporally averaged Fourier amplitude squares versus the wave vector components k_ξ, k_η. The lattice size is 64×64, the other data are as in Fig. 2.

inertial coupling contribution increases quicker than the dissipative one because $|\nu_1| > |\nu_2|$, see equation (8). So the scaling intrinsic to inertial coupling will be observed in any asymptotically small vicinity of the critical point $\{\lambda = \lambda_c,\ \varepsilon = 0\}$. This conclusion agrees with the self-similarity of the stability regions found by Kapral [3] for spatially uniform states with different temporal periods. This structure is reproduced under a scale change by δ and a along the coordinate axes λ and ε, respectively.

Our formulation of scaling properties is somewhat more substantial. It relates not only to infinitesimal perturbations of uniform states but also to arising spatial structures with finite amplitudes. Furthermore, we conclude that the linear coupling is not the best example to demonstrate the scaling property. Choosing the proper relation between the coupling parameters in equation (11), namely $\varepsilon_1 = \varepsilon$, $\varepsilon_2 = 0.088\varepsilon$ [see (12)], we obtain the lattice with pure inertial coupling:

$$x_{n+1}(i, j) = f(x_n(i, j)) + (\varepsilon/4)\{[x_n(i+1, j) + x_n(i-1, j) + x_n(i, j+1) + x_n(i, j-1) - 4x_n(i, j)] + 0.088[f(x_n(i+1, j)) + f(x_n(i-1, j)) + f(x_n(i, j+1)) + f(x_n(i, j-1)) - 4f(x_n(i, j))]\}.$$

Figures 4 and 5 show the snapshot patterns of this lattice 32×32 with periodic boundary conditions and random initial conditions. The rules of rescaling for parameters and initial conditions are the same as in the previous case except for the coupling parameter. Now we take $\varepsilon \to \varepsilon/a^K$, where K is the scaling level. Figure 4 shows the checkerboard patterns arising in the subcritical region. They are demarcated by the strings, which are almost motionless here. Figure 5 presents the phases of developed turbulence. Visual comparison of the pictures in Figs 4 and 5 supports the expected scaling because the same character of patterns is observed at different levels. For quantitative verification, the maximal Lyapunov exponent and spatial spectra were calculated for the regimes corresponding to Fig. 5. The Lyapunov exponents are presented in Table 1. One can see again the coincidence of $L \cdot 2^K$

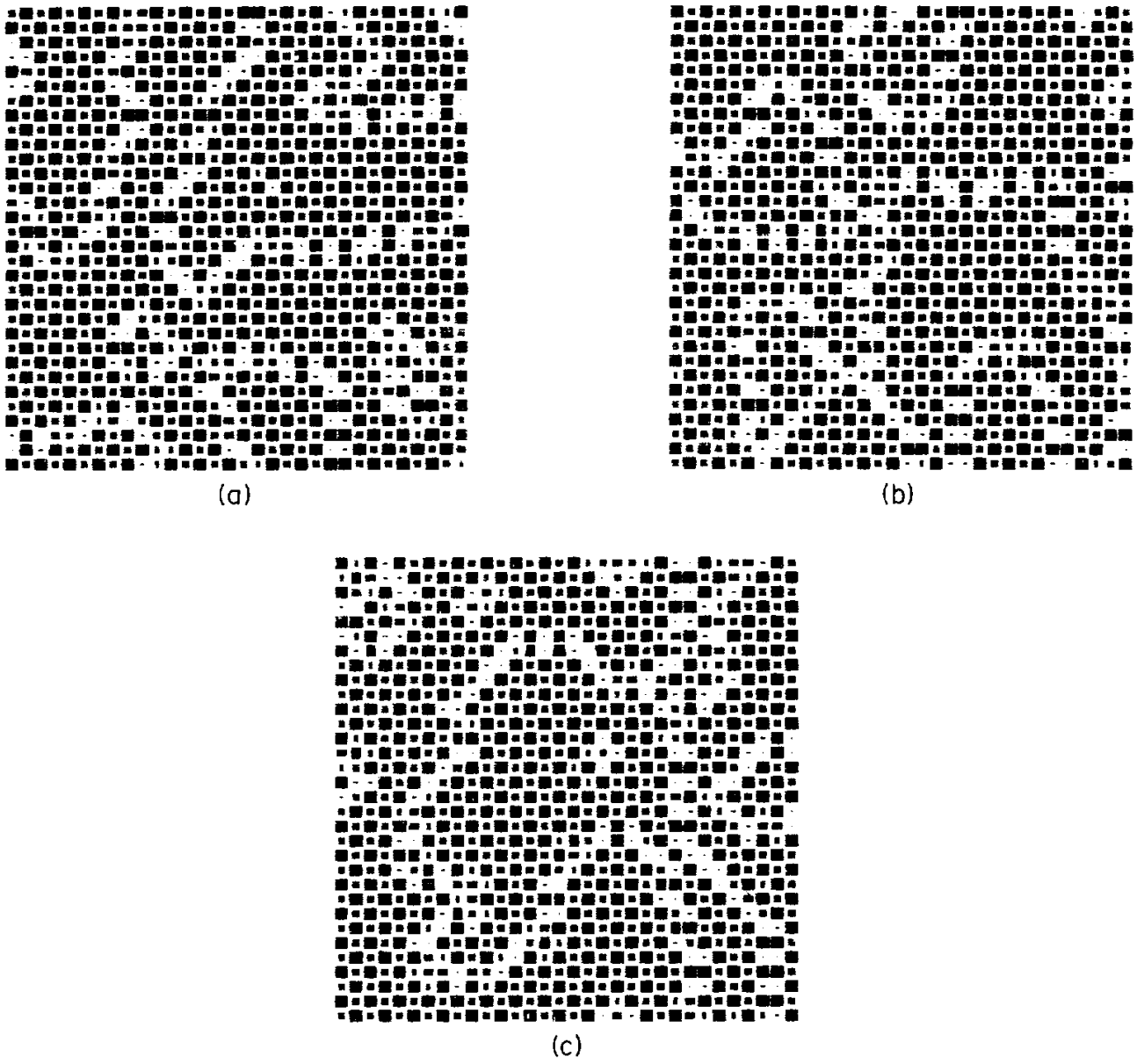

Fig. 4. Checkerboard domains demarcated by string type defects in the lattice, size 32×32 with pure inertial coupling [equation (11) with $\varepsilon_2 = 0.088\varepsilon_1$] at three levels of the lattice scaling K. The values $x(i, j)$ are coded by squares of size $\propto [a^K x(i, j) - 0.1]$; (a) $K = 0$, $\lambda = 1.05$, $\varepsilon_1 = -0.4$, the random initial condition amplitude $\Delta x_{\mathrm{rnd}} = 0.4$, the iteration number $n = 64$, (b) $K = 1$, $\lambda = 1.325948$, $\varepsilon = 0.15981$, $\Delta x_{\mathrm{rnd}} = 0.16$, $n = 128$, (c) $K = 2$, $\lambda = 1.385048$, $\varepsilon = -0.06385$, $\Delta x_{\mathrm{rnd}} = 0.064$, $n = 256$.

values for different levels K. The spatial spectra (calculated for the lattice 64×64) also satisfy the scaling property (see Fig. 6).

In conclusion of this section we demonstrate the scaling property for the case of arbitrary composite coupling. To find the renormalization rule for the coupling constants ε_1, ε_2 we calculate the inertial and dissipative coupling parameters C_1, C_2 from equation (12). Then they are rescaled as $C_1 \to C_1/a^K$, $C_2 \to C_2/2^K$, and the new ε_1, ε_2 are defined from the inverse of equation (12):

$$\varepsilon_1 \to \varepsilon_1/a^K, \ \varepsilon_2 \to \varepsilon_2/2^K + 0.088\varepsilon_1(1/a^K - 1/2^K).$$

We choose the particular set of parameters $\lambda = 1.54$, $\varepsilon_1 = 0.36$, $\varepsilon_2 = 0.3$ and a random initial condition amplitude of 0.4 at zero level. For the levels $K = 0, 1, 2$, the snapshot patterns are shown in Fig. 7 using the above stated rules of visualization, the spatial spectra are compared in the semilog plot of Fig. 8. The Lyapunov exponents L and $L \cdot 2^K$ values

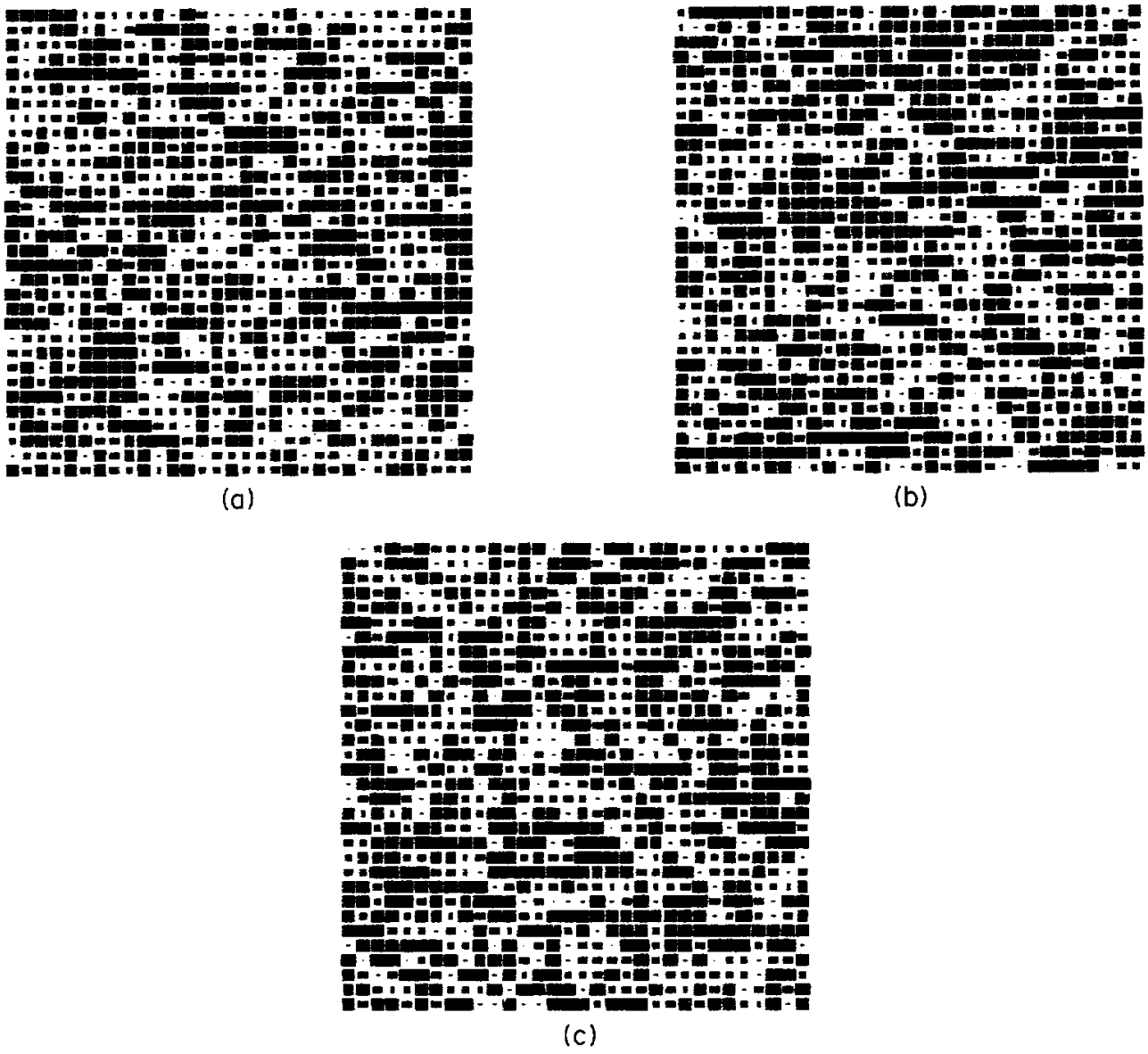

Fig. 5. Snapshot diagrams showing developed turbulence in the lattice, size 32×32 with pure inertial coupling for three levels of the lattice scaling K. The values $x(i, j)$ are coded by squares of size $\propto [a^K x(i, j) + 1]$; (a) $K = 0$, $\lambda = 1.54$, $\varepsilon_1 = 0.1$, the random initial condition amplitude $\Delta x_{\text{rnd}} = 0.4$, the iteration number $n = 64$, (b) $K = 1$, $\lambda = 1.430892$, $\varepsilon_1 = -0.039953$, $\Delta x_{\text{rnd}} = 0.16$, $n = 128$, (c) $K = 2$, $\lambda = 1.407524$, $\varepsilon_1 = 0.015963$, $\Delta x_{\text{rnd}} = 0.064$, $n = 256$.

are presented in the last block of the Table 1. So we see that the lattice scaling property is satisfactorily fulfilled in all considered cases.

RENORMALIZATION GROUP, UNIVERSALITY AND SCALING IN THE CONTINUOUS LIMIT

Let us turn now to the situation when the dynamics of CML may be considered in the continuous limit, i.e. one can use continuous spatial variables ξ, η instead of discrete indices i, j. It restricts the approach to CML with dominating diffusive coupling but leads to more far-reaching conclusions about spatio-temporal dynamics near the onset of chaos. For this case we develop the revised version of RG including rescaling of spatial coordinates.

We begin with the consideration of the dissipatively coupled map lattice [see equation (10)] at the Feigenbaum critical point $\lambda = \lambda_c$ and we suppose the coupling parameter ε to

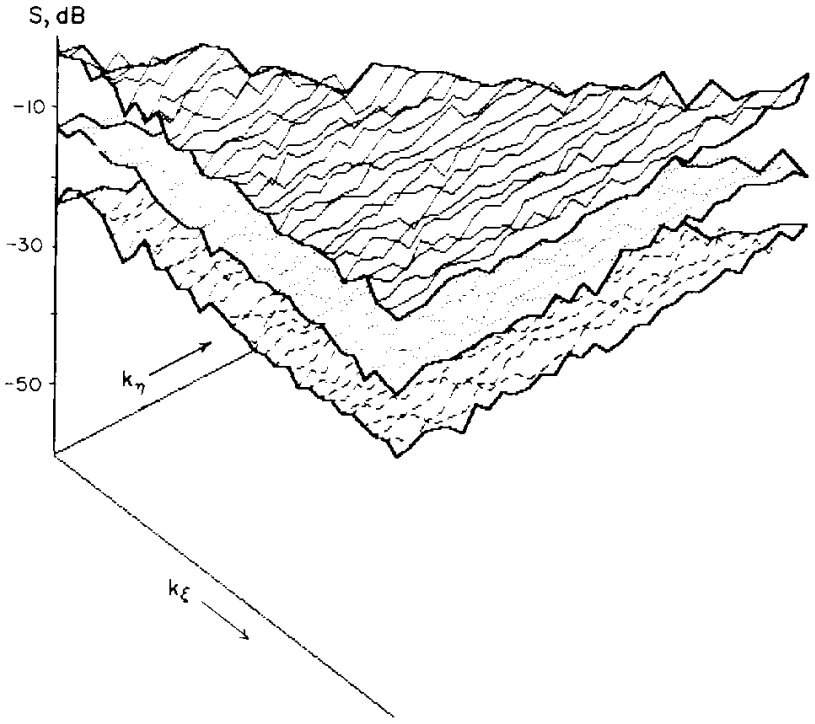

Fig. 6. Spatial spectra for three turbulent states similar in the sense of the lattice scaling: logarithm of temporally averaged Fourier amplitude squares versus the wave vector components k_ξ, k_η. The lattice size is 64×64, the other data are as in Fig. 5.

be small. Then, let us perform the RG procedure from the previous section many times. At each new step we deal with the states concentrated in a narrower interval of the dynamical variable ($u \propto 1/a^K$) while the effective coupling parameter increases as $\varepsilon \cdot 2^K$. For sufficiently large K the linear approximation (8) fails. However, it is quite reasonable to suppose that in the situation of extremely strong influence of dissipative coupling patterns would only arise where there is a very small difference between the neighbour cells. Returning to the description of the situation by the initial dynamical equation, we can define continuous spatial variables $\xi = 2i/\sqrt{\varepsilon}$, $\eta = 2j/\sqrt{\varepsilon}$ and change the difference term to Laplacian:

$$x_{n+1}(\xi, \eta) = f(x_n(\xi, \eta)) + \left(\frac{\partial^2}{\partial \xi^2} + \frac{\partial^2}{\partial \eta^2}\right) f(x_n(\xi, \eta)). \tag{14}$$

Now, rescaling the coupling parameter by two is equivalent to rescaling the spatial variables by $\sqrt{2}$. So we can redefine the RG transformation. Now the fixed point operator will correspond to a distributed coupled map medium with diffusion rather than to an uncoupled map lattice.

Let us consider this development of the approach in detail. Denoting the initial evolution operator by $G_0[x]$ we use this operator twice and make scale change $\hat{S}x(\xi, \eta) = au(\xi\sqrt{2}, \eta\sqrt{2})$. Then the new operator $G_1[x] = \hat{S}G_0G_0\hat{S}^{-1}[x]$ is obtained for evolution over two temporal steps. By repeating this procedure many times, we come to the recurrent operator equation

$$G_{K+1}[x] = \hat{S}G_KG_K\hat{S}^{-1}[x], \tag{15}$$

where G_k is the renormalized evolution operator for 2^K temporal steps.

We believe that the following statements are valid.

1. Let the initial operator G_0 be the evolution operator obtained in the continuous limit for a spatially extended lattice constructed by period doubling cells with dissipative

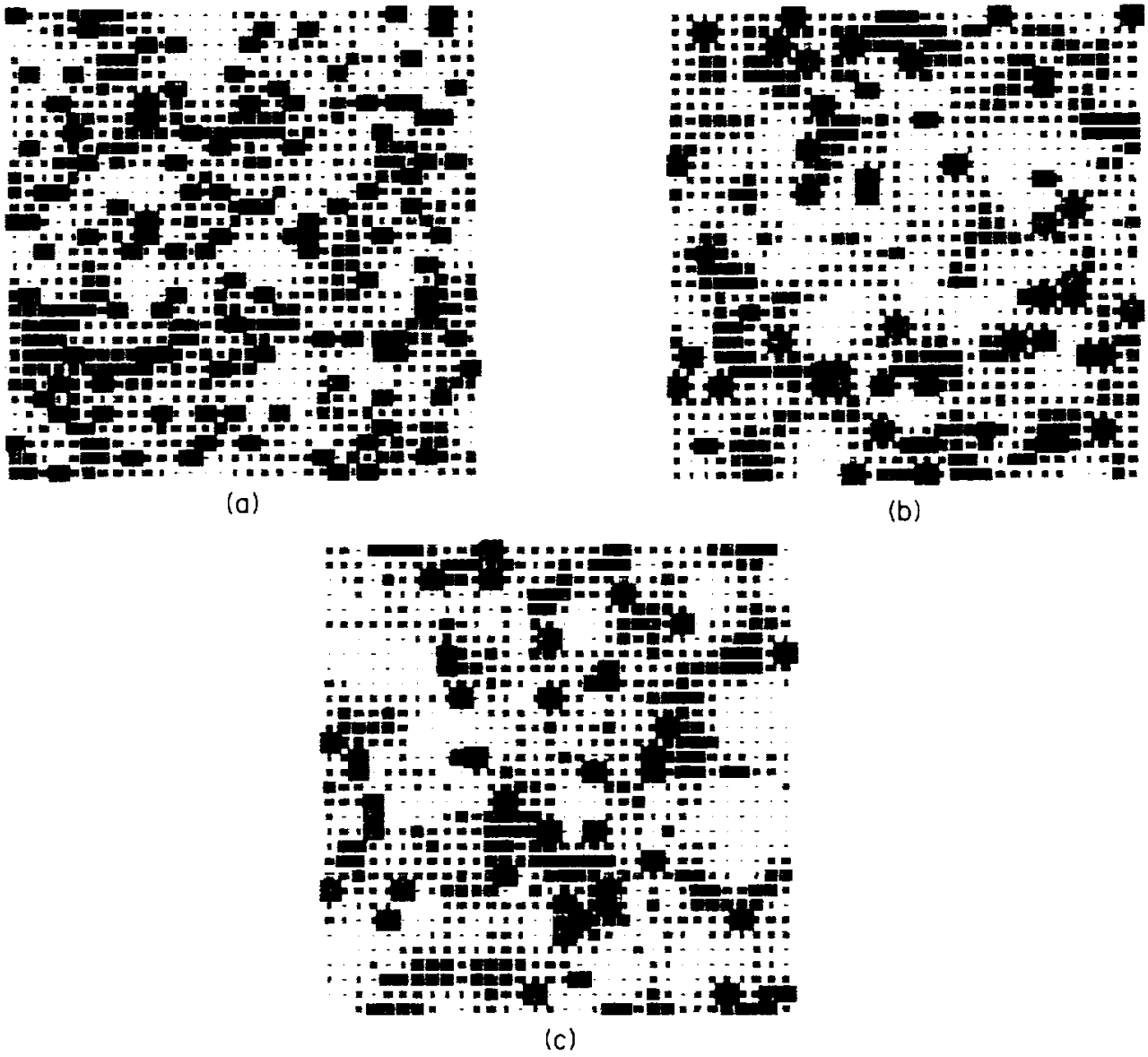

Fig. 7. Snapshot diagrams illustrating the lattice scaling for three levels K in the lattice, size 32×32 with composite coupling [equation (11)]. The values $x(i, j)$ are coded by squares of size $\propto [a^K x(i, j) + 0.4]$: (a) $K = 0$, $\lambda = 1.54$, $\varepsilon_1 = 0.36$, $\varepsilon_2 = 0.3$, the random initial condition amplitude $\Delta x_{\text{rnd}} = 0.4$, the iteration number $n = 224$, (b) $K = 1$, $\lambda = 1.430892$, $\varepsilon_1 = -0.14383$, $\varepsilon_2 = 0.12150$, $\Delta x_{\text{rnd}} = 0.16$, $n = 448$, (c) $K = 2$, $\lambda = 1.407524$, $\varepsilon_1 = 0.05747$, $\varepsilon_2 = 0.07214$, $\Delta x_{\text{rnd}} = 0.064$, $n = 892$.

coupling. Then, for the critical value of the cell control parameter, the sequence of operators generated by equation (15) converges to the regular limit G. This operator is the fixed point of the RG equation

$$G[x] = \hat{S} G G \hat{S}^{-1}[x] \tag{16}$$

2. The operator G is universal, i.e. it is the same for a wide class of the systems with dissipative coupling between the spatial elements. The only difference may be in characteristic scales for x and ξ, η.

The equations (15) and (16) have the form supposed earlier by Kuznetsov and Pikovsky [5] for one-dimensional systems, but here all the operators act in the space of two argument functions.

We notice that the considered model (10) admits factorization in the form

$$x_{n+1}(i, j) = \hat{L} f(x_n). \tag{17}$$

It isn't an accidental circumstance. It may be shown that the possibility of such

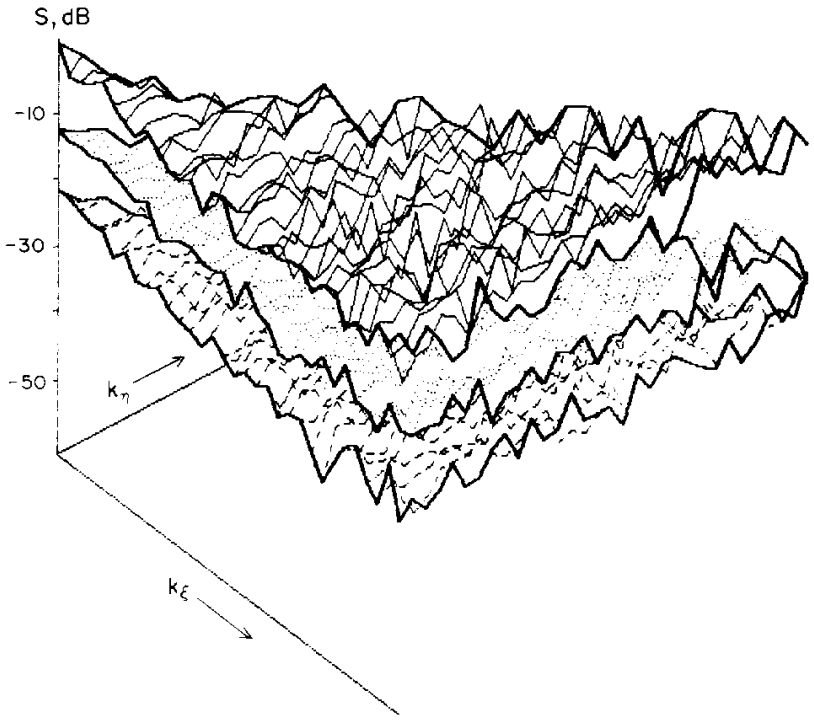

Fig. 8. Spatial spectra for three turbulent states similar in the sense of the lattice scaling: logarithm of temporally averaged Fourier amplitude squares versus the wave vector components k_ξ, k_η. The lattice size is 64×64, the other data are as in Fig. 7.

representation is a sufficient condition for the system to belong to the universality class associated with the fixed point G. Notice that the map f must exhibit the Feigenbaum period doublings, and the linear operator $\hat{L}$ must satisfy the following requirements:

1. Translation invariance: the operator may be represented in general as $\hat{L}x(\xi, \eta) = \int\int C(\xi', \eta')x(\xi - \xi', \eta - \eta')\mathrm{d}\xi'\mathrm{d}\eta'$.
2. Normalization: $\int\int C(\xi, \eta)\mathrm{d}\xi\mathrm{d}\eta = 1$.
3. Locality: the integral $\Delta^2 = (1/4)\int\int(\xi^2 + \eta^2)C(\xi, \eta)\mathrm{d}\xi\mathrm{d}\eta$ is finite. The value Δ defines the characteristic spatial scale for the operator $\hat{L}$—diffusion length per temporal step.
4. Local isotropy of the spectrum and dissipativity: the spectrum $L(k, q) = \mathrm{e}^{-ik\xi - iq\eta}\hat{L}\mathrm{e}^{ik\xi + iq\eta} = 1 - \Delta^2(k^2 + q^2) + o(k^2, q^2)$ and $|L(k, q)| < 1$ for all $k, q \neq 0$.

We don't give here the mathematically rigorous proof for the formulated statements, but we shall demonstrate the convincing results of its numerical verification. The following procedure is performed for several values of K. We take the CML (10) containing M_K cells with periodic boundary conditions. Here $M_0 = 26$ is an arbitrary chosen integer and M_K is the integer nearest to $2^{K/2}M_0$. Then, we take the ensemble of probe functions U, $|U| \leq 1$. These functions may be given as the linear combination of standing waves with random amplitudes and phases

$$U(i, j) = \sum A_{pq} \cos(2\pi ip/M_K + \phi_i) \cos(2\pi jq/M_K + \phi_j).$$

Then, we give the initial condition $x(i, j) = U(i, j) \cdot a^{-K}$ and iterate the equation (10) by 2^K times. We show the end states in Fig. 9 (a) and (b) for two representatives of the ensemble $\{U\}$ using the normalization $X = i/M_K$, $Y = j/M_K$, $Z = xa^K$. These are just the plots of the functions $G_K[U]$ vs the spatial variables. One can see an excellent convergence of supposed data for $K = 3, 4, 5$. It was also valid for larger K with increasing accuracy, but addition of the data would make the picture illegible. The limit for $K \to \infty$ corresponds to the result of action of the fixed point operator G on the probe function U.

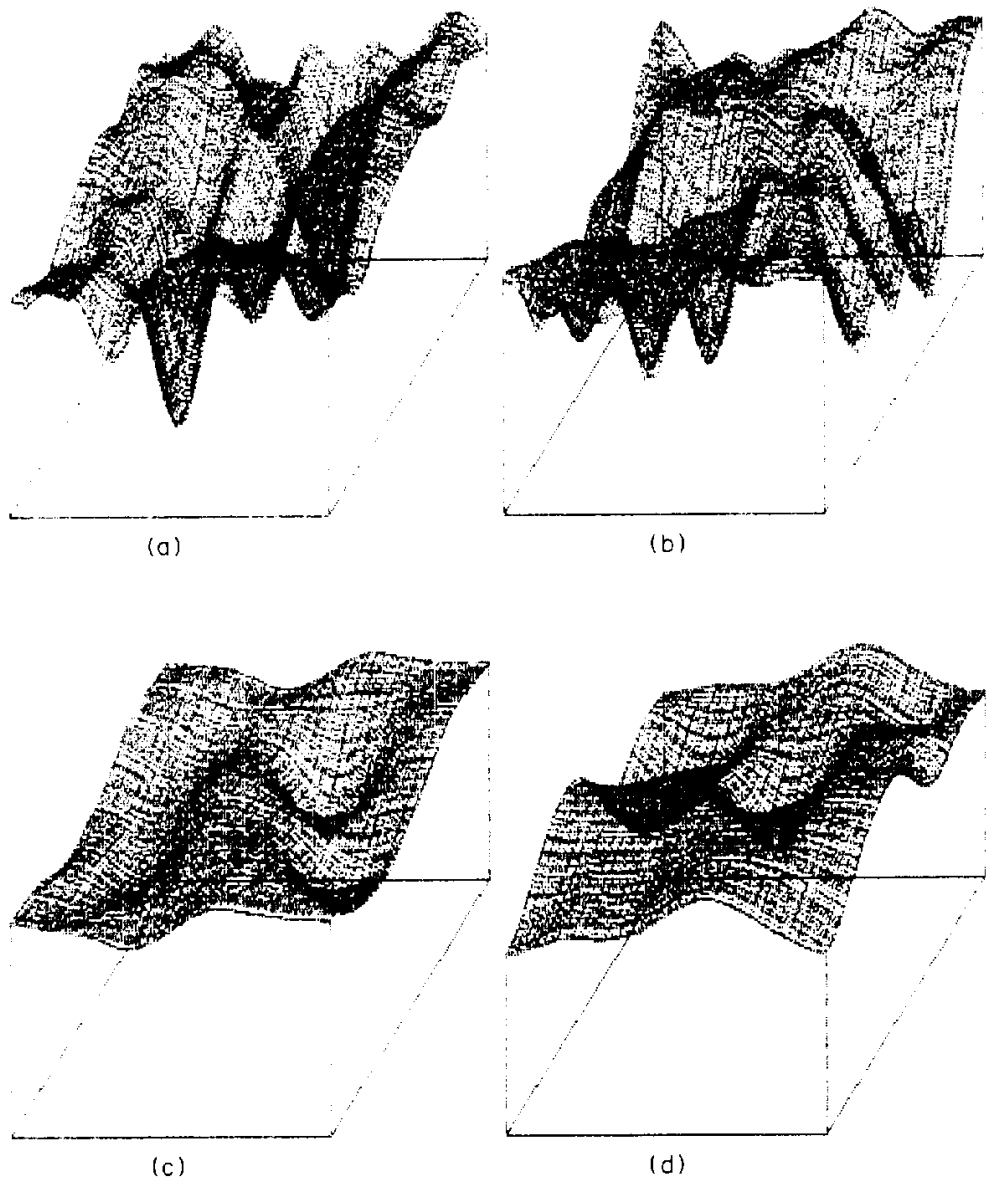

Fig. 9. Numerical verification of the existence and universality of the fixed point operator G responsible for continuous scaling in the dissipatively coupled lattices. The control parameter value is the limit point of period doublings of a local map λ_c: (a, b)—results of 8, 16 and 32 iterations of equation (10) with $\varepsilon = 0.4$, the lattice sizes are 26×26, 37×37 and 52×52, respectively, for two probe functions, with the use of renormalization rules formulated in the text; (c, d)—results of 16 iterations for two probe initial functions and three different lattice models, where the averaging operator over 5, 9 and 13 neighbours was taken as operator $\hat{L}$ in equation (17). The lattice sizes are 27×27, 35×35 and 44×44, respectively.

In the same manner one can verify the universality. The above scheme of calculations is reproduced for several different systems (17). For example, we consider the different forms of operator $\hat{L}$ averaging the states over five, nine and thirteen neighbour cells. The values of diffusive lengths Δ are $1/\sqrt{5}$, $1/\sqrt{3}$, $\sqrt{7/13}$, and we choose the lattice size to make the M/Δ value approximately equal for all the cases: $M = 27$, 35 and 44, respectively. The results of calculations for sufficiently large $K = 4$ are presented in Fig. 9 (c) and (d) for three systems. One can see that the superposed configurations coincide very well in accordance with our hypothesis of the universality.

Following the logic of the RG approach, we must turn now to the analysis of solutions for RG equation (15) near the fixed point G. Substituting $G_n[x] = G[x] + \varepsilon h_n[x]$ into (15) and supposing $\varepsilon \ll 1$, we obtain the operator equation

$$h_{n+1}[x] = \hat{S}G'(G\hat{S}^{-1}[x])h_n\hat{S}^{-1}[x] + \hat{S}h_nG\hat{S}^{-1}[x], \tag{18}$$

where $G'(G\hat{S}^{-1}[x])$ is the Frechet derivative of the operator G. The last equation has a structure $h_{n+1}[x] = \hat{M}h_n[x]$, where $\hat{M}$ is the linear operator. One may expect that the asymptote of the solution h_n will be defined by the superposition of the operator $\hat{M}$ eigenvectors with the largest magnitudes of eigenvalues. Fortunately, these eigenvalues as well as the necessary information about the structure of the eigenvectors may be found without formal solution of the operator eigenproblem.

Let us return to the universal representation of the evolution operator near the lattice fixed point given by equation (7) and assume that the dissipative coupling dominates:

$$C_1 \ll C_2 \ll 1 \tag{19}$$

Now we can choose one of two ways.

1. To replace differences by spatial derivatives in equation (7) immediately and then to perform the RG transformation (15) n and $n+1$ times. Due to the inequality (19) it is possible to choose n to provide the operators $G_n = G + Ah_n$ and $G_{n+1} = G + Ah_{n+1}$ close to the fixed point G.

2. Preliminary to perform the lattice RG transformation (2), then introduce the continuous spatial variables and rescale them by $\sqrt{2}$. The dissipative-type term isn't changed after this procedure, while the inertial-type term accepts the factor $a/2$. Then we perform the RG transformation (15) n times and obtain the operator $\tilde{G}_n = G + Ah_n a/2$, which must coincide with the above operator G_{n+1}. So, we have $h_{n+1} = h_n a/\sqrt{2}$. Thus, the operator that arises from the considered initial perturbation is just the eigenvector of equation (26) with the eigenvalue $\nu_1 = a/2 = -1.2512\ldots$ We denote this eigenvector by H_1. Of course, the eigenvector H_0 must be added corresponding to perturbation of the local map parameter, with eigenvalue $\nu_0 = \delta = 4.6692\ldots$.

Now we give the formulation of the *continuous scaling*.

In the continuous limit the spatially distributed system with dominating diffusion is characterized by two essential parameters Λ and a,—the factors at the eigenvectors H_0 and H_1. The parameter space $\{\Lambda, a\}$ has the property of the scale invariance under parameters change $\Lambda \to \Lambda/\delta$, $a \to a/\nu_1$. This change is accompanied by doubling the temporal scale of similar states, increasing the spatial scale by $\sqrt{2}$ and rescaling the dynamical variable x by $1/a$.

This formulation relates to the infinite size system. One may also find the similar states in the case of a system of finite size, but an additional parameter, the spatial size M, must be taken into account with the renormalization rule $M \to M\sqrt{2}$.

It is easy to write the continuous limit form of the universal model by adding the inertial coupling term in equation (14). Supposing the form $f(x) = 1 - \lambda x^2$ for the local map and taking the proper ratio of linear and quadratic couplings in the added term [see equation (12)], we have

$$x_{n+1}(\xi, \eta) = f(x_n(\xi, \eta)) + \left(\frac{\partial^2}{\partial\xi^2} + \frac{\partial^2}{\partial\eta^2}\right) f(x_n(\xi, \eta)) \tag{20}$$
$$+ a\left(\frac{\partial^2}{\partial\xi^2} + \frac{\partial^2}{\partial\eta^2}\right)(x_n(\xi, \eta) + 0.088 f(x_n(\xi, \eta))).$$

However, the lattice model of equation (11) remains more suitable for computer experiments to demonstrate and verify the continuous scaling properties. We must only formulate the rules of renormalization in terms of parameters presented in this equation. We find the inertial and dissipative coefficients from equation (12), renormalize them by $C_1 \to C_1(a/2)^{-K}$, $C_2 \to C_2$ and return to the ε parameters using the inverse of equation (12):

$$\varepsilon_1 \to \varepsilon_1(a/2)^{-K},\ \varepsilon_2 \to \varepsilon_2 - 0.088\varepsilon_1 + 0.088\varepsilon_2(a/2)^{-K}.$$

The *unique* relevant parameter λ remains in the case of *pure dissipative coupling*. Transition to the Kth scaling level is provided by rescaling of this parameter without change of coupling. Notice that the sustained dynamics of an asymptotically large system in the continuous limit seems to be independent of the size parameter M and of the random initial condition amplitude (except that too large amplitudes lead to divergence). The dynamics in the subcritical region consists of the squeezing and disappearance of the domains that existed due to initial conditions and leads to uninteresting uniform states. Thus, our computer examples will relate to supercritical λ.

Let us explain briefly how the suitable lattice size M must be chosen. We emphasize that the required M value increases when we come toward the critical point λ_c. Really, $\lambda - \lambda_c$ behaves as δ^{-K} and M as $2^{K/2}$ with dependence on the scaling level K. So, $M \propto (\lambda - \lambda_c)^{-\nu}$, where $\nu = (1/2)\log_\delta 2 = 0.2249\ldots$. Hence, we may write the evaluation for the 'coherence length' of the threshold size, when the system begins demonstrate the dynamics intrinsic to the infinite one:

$$L_{coh} = C\sqrt{\varepsilon}(\lambda - \lambda_c)^{-\nu},$$

The factor C may be evaluated from the data found by Bohr and Christensen [9]; in our normalization $C \simeq 7$. We fix the system size sufficiently large to satisfy the condition $M > L_{coh}$ for all considering scaling levels $K < K_{max}$.

Figure 10 shows the snapshot diagrams for similar (in the continuous scaling sense) turbulent states of the lattice model (10) with $\varepsilon = 0.4$. The periodic boundary conditions were used for the lattice 60×60. The initial conditions were given by the random numbers of small amplitude. The pictures were observed at each 16th temporal step up to the appearance of the visually unchanging character of turbulent patterns. At the scaling level $K = 0$ we take $\lambda = 1.54$, which is rescaled for $K = 1, 2, 3$ according to the rule $\lambda \to \lambda_c + (\lambda - \lambda_c)/\delta^k$. The values of $x(i, j)$ are coded by squares of size proportional to $[a^k x(i, j) + 0.4]$.

Comparing Figs 10 (a–d), one can see that they look like subsequently magnified

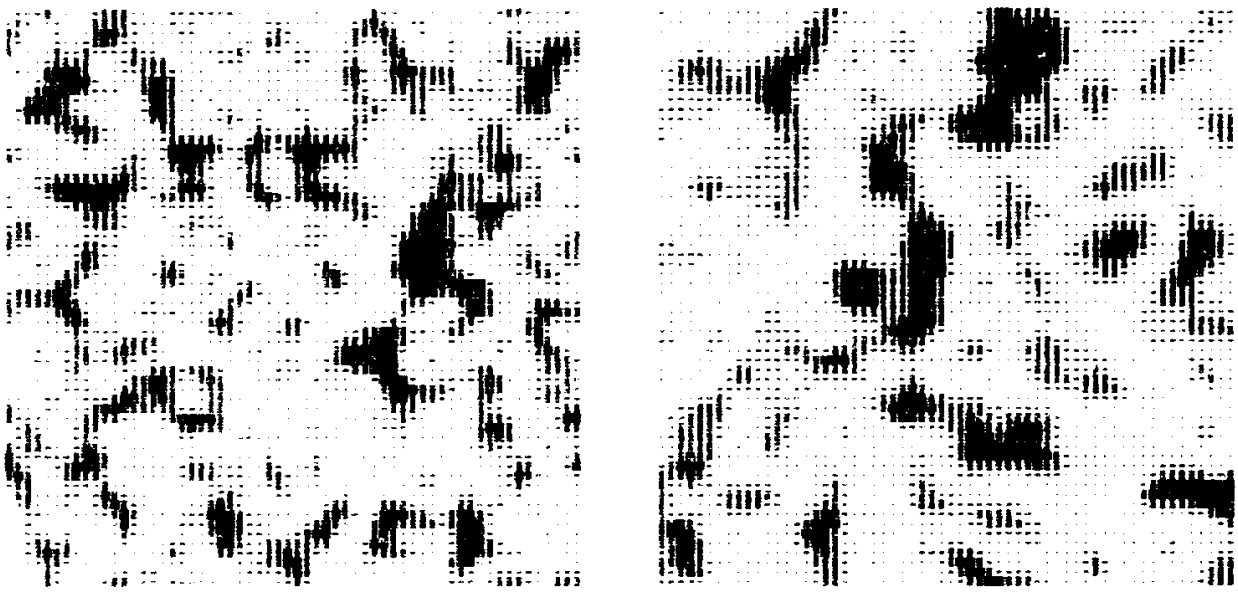

(a) (b)

Fig. 10(a) and (b). Caption on p. 297.

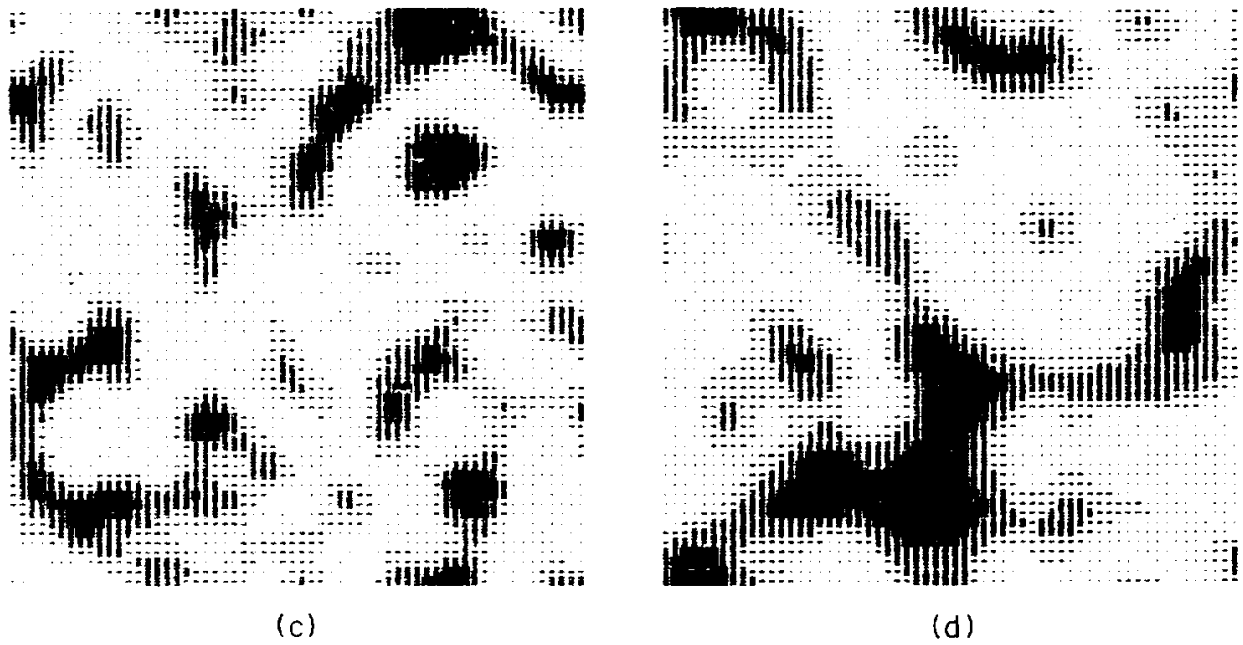

Fig. 10. Snapshot diagrams illustrating the continuous scaling for four levels K in the dissipatively coupled lattice, size 60×60, [equation (10)] with periodic boundary conditions, $\varepsilon = 0.4$. The values $x(i, j)$ are coded by squares of size $\propto [a^K x(i, j) + 0.4]$; (a) $K = 0$, $\lambda = 1.54$, (b) $K = 1$, $\lambda = 1.430892$, (c) $K = 2$, $\lambda = 1.407524$, (d) $K = 3$, $\lambda = 1.402519$.

pictures of the same turbulent structure. This observation qualitatively supports the expected scaling property.

The spatial spectra were calculated for the lattice 64×64 by the same algorithm as in previous section, but without change of coupling for different K. The lattice is isotropic in the continuous limit, so the spectra at high scaling levels must depend only on the modulus of the wave vector k. They are depicted in Fig. 11 using the log–log plot. One can see the reproduction of the spectra shapes from one level to another with constant vertical and horizontal shifts reflecting the scale renormalization for dynamical variable and spatial coordinates. At last, the Lyapunov exponents L are presented in Table 2 for the same regimes. $L \cdot 2^K$ value independence of the scaling level K (within the accuracy of calculations) shows that the scaling property really works.

Figures 12 and 13 show the snapshot diagrams and spatial spectra obtained for the lattice (11). At the level $K = 0$ we take $\lambda = 1.54$, $\varepsilon_1 = 0.36$, $\varepsilon_2 = 0.3$. The other conditions and

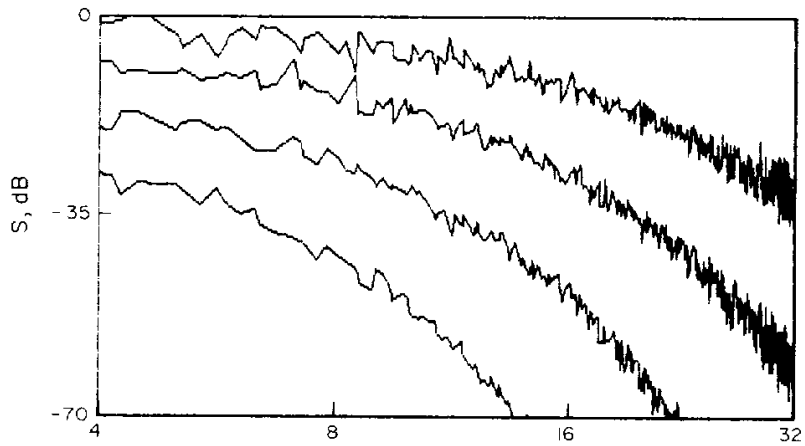

Fig. 11. Spatial spectra for three turbulent states similar in the sense of the continuous scaling: logarithm of temporally averaged Fourier amplitude squares versus logarithm of the wave vector modulus. The lattice size is 64×64, the other data are as in Fig. 10.

Table 2. The maximal Lyapunov exponent L for states of the model (11) similar in the sense of the continuous scaling. The type of coupling: pure dissipative (upper block), composite (lower block). The lattice size is 32×32, periodic boundary conditions

K	λ	ε_1	ε_2	L	$L \cdot 2^K$
0	1.540000	0	0.4	0.144 ± 0.008	0.144 ± 0.008
1	1.430892	0	0.4	0.074 ± 0.004	0.147 ± 0.008
2	1.407524	0	0.4	0.036 ± 0.002	0.146 ± 0.008
0	1.540000	0.36	0.3	0.096 ± 0.008	0.096 ± 0.008
1	1.430892	−0.28767	0.24301	0.060 ± 0.004	0.119 ± 0.008
2	1.407524	0.22987	0.28855	0.030 ± 0.002	0.122 ± 0.008

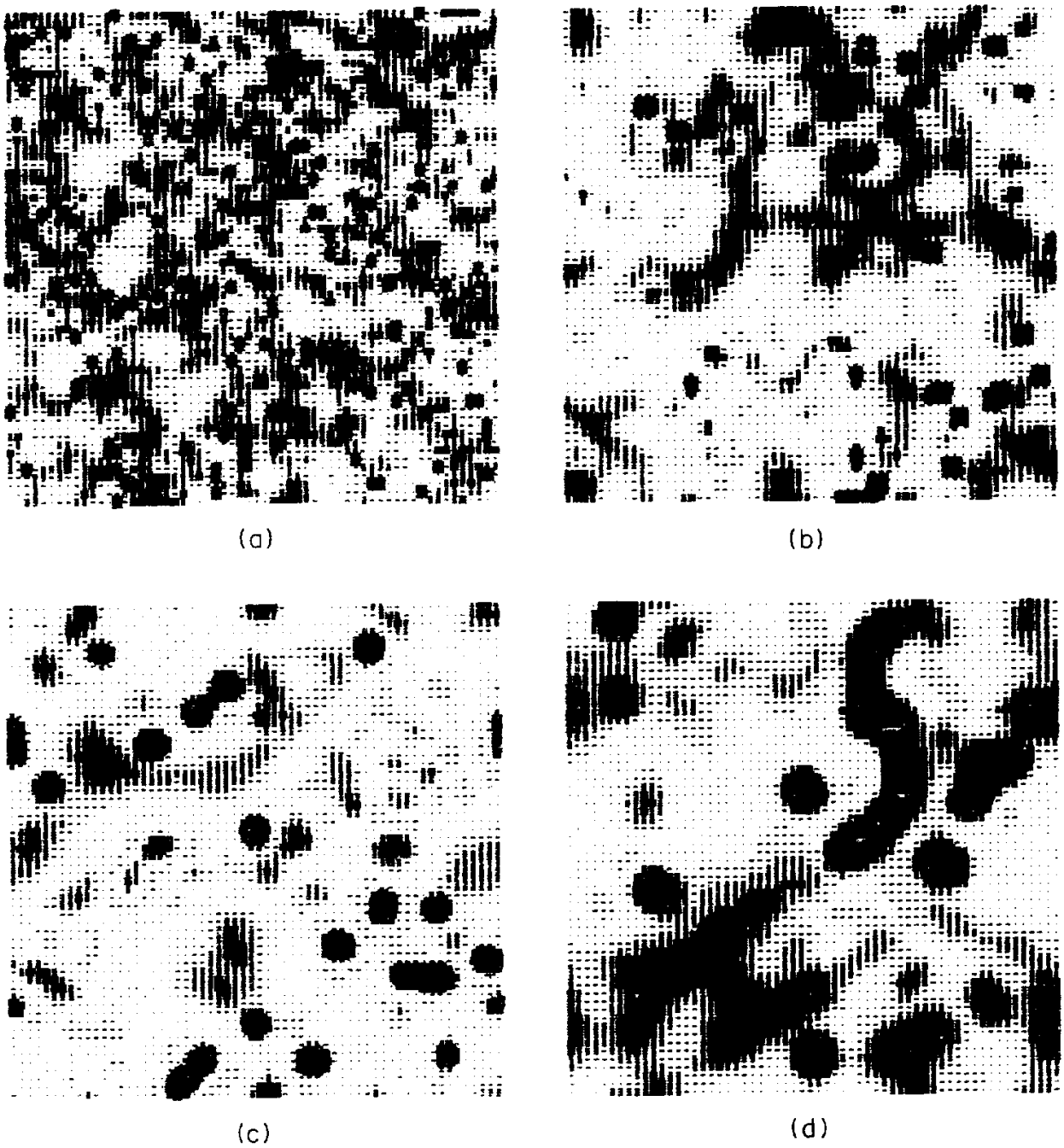

Fig. 12. Snapshot diagrams illustrating the continuous scaling for four levels K in the lattice, size 60×60, with composite coupling [equation (11)]. The values $x(i, j)$ are coded by squares of size $\propto [a^K x(i, j) + 0.4]$; (a) $K = 0$, $\lambda = 1.54$, $\varepsilon_1 = 0.36$, $\varepsilon_2 = 0.3$, (b) $K = 1$, $\lambda = 1.430892$, $\varepsilon_1 = -0.28767$, $\varepsilon_2 = 0.24301$, (c) $K = 2$, $\lambda = 1.407524$, $\varepsilon_1 = 0.22987$, $\varepsilon_2 = 0.28855$, (d) $K = 3$, $\lambda = 1.402519$, $\varepsilon_1 = -0.17368$, $\varepsilon_2 = 0.25216$.

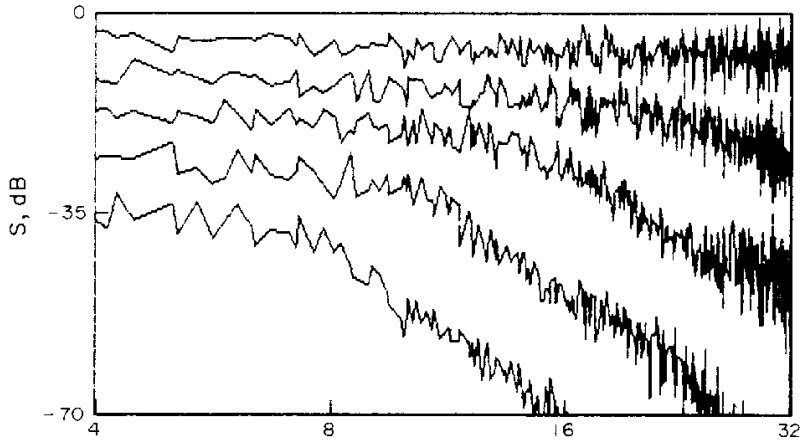

Fig. 13. Spatial spectra for three turbulent states similar in the sense of the continuous scaling: logarithm of temporally averaged Fourier amplitude squares versus logarithm of the wave vector modulus. The lattice size is 64×64, the other data are as in Fig. 12. At the last scaling level $K = 4$, $\lambda = 1.401447$, $\varepsilon_1 = 0.14677$, $\varepsilon_2 = 0.28124$.

methods of representation remain the same as for Figs 10 and 11 discussed above. Also the Lyapunov exponents L and $L \cdot 2^K$ values are presented in Table 2 for scaling levels $K = 0$, 1, 2. Again we see the manifestation of scaling with very high accuracy (except at the lowest level).

CONCLUSIONS

The presented RG approach plays a similar role to the two-dimensional CML as the Feigenbaum theory for the ordinary period-doubling systems. Notice that it leads to the important idea of scaling properties for spatial patterns.

Two proposed versions of RG analysis, lattice and continuous, give us an example of the coexistence of two critical situations with different codimensions in the CML parameter space. Figure 14 explains a relation between the lattice and continuous scaling for the simplest case of the system with pure diffusion. The critical point L associated with the fixed point of the lattice RG transformation exists in the plane of the control parameter vs the coupling constant. Also the critical line C exists, where the long time evolution

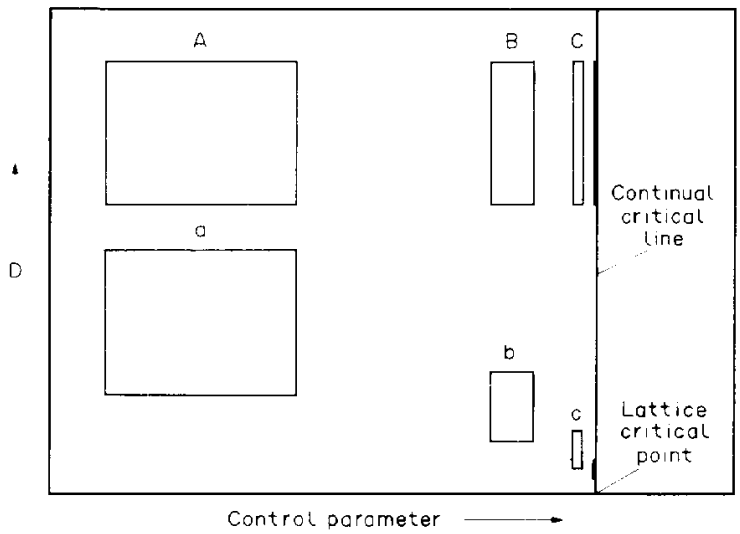

Fig. 14. Explanation of the relation between the lattice and continuous scaling for the CML with pure diffusion. The sequences of the regions are shown similar in a sense of the first (a, b, c, ...) and the second (A, B, C, ...) type of scaling.

operators converge to the universal operator G. Two sets of regions are shown which are similar in the sense of the lattice scaling (a, b, c) and in the sense of the continuous one (A, B, C).

In general, the search for, and classification of various critical behaviour types according to their codimensions seems to be a promising direction in nonlinear dynamics.

We emphasize the principal importance of two coupling types, inertial and dissipative, for understanding CML dynamics near the onset of chaos. In spite of familiar terminology, their nature is significant because it arises from the structure of the RG, not from some artificial construction. Due to universality of the coupling types, the lattice models were defined with a few control parameters, giving the full variety of phenomena intrinsic to the corresponding universality class. The construction of such models must be considered as a separate important problem of the theory.

The RG analysis throws light on possible CML applications in order to describe real systems. Now, the CMLs may be considered not only as qualitative illustrations of turbulent behaviour, but also as legal representatives of their universality classes, suitable for quantitative description of the phenomena near the onset of chaos.

We believe that our approach gives the adequate theoretical grounding to a number of scaling properties observed earlier by Kapral, Oppo and Kapral and Bohr and Christensen [3, 7, 9]. Being essentially different for linear and quadratic couplings, they are now treated from a common point of view.

Notice, that increasing the characteristic spatial scale near the continuous scaling critical situation has a straightforward analogy in phase transition theory: the correlation length increasing near the critical temperature. In general, development of the RG approach including the spatial variables promotes the convergence of concepts of the dynamical system theory and the phase transition theory.

One may hope that results of this work would favour the statement of experimental investigations guided by the concept of RG, universality and scaling.

REFERENCES

1. K. Kaneko, Period doubling of kink–antikink patterns, quasiperiodicity in antiferrolike structures in coupled logistic lattice, *Prog. Theor. Phys.* **72**(3), 480–486 (1984).
2. I. Waller and R. Kapral, Spatial and temporal structure in systems of coupled nonlinear oscillators, *Phys. Rev.* **A30**(4), 2047–2055 (1984).
3. R. Kapral, Pattern formation in two-dimensional arrays of coupled discrete time oscillators, *Phys. Rev.* **A31**(6), 3868–3879 (1985).
4. S. P. Kuznetsov, On model description of coupled dynamical system near the transition point order–disorder, *Izv. Vuzov. Fiz.* **27**(6), 87–96 (1984).
5. S. P. Kuznetsov and A. S. Pikovsky, Universality and scaling of period-doubling bifurcations in a dissipative distributed medium, *Physica* **D19**(3), 384–396 (1986).
6. S. P. Kuznetsov, Renormalization group, universality and scaling in dynamics of one-dimensional auto-wave media, *Radiophys. Quant. Elect.* **29**(8), 679–692 (1986).
7. J. -L. Oppo and R. Kapral, Discrete models for the formation and evolution of spatial structure in dissipative systems, *Phys. Rev.* **A33**(6), 4219–4231 (1986).
8. I. S. Aranson, A. V. Gaponov-Grekhov and M. I. Rabinovich, The onset and spatial development of turbulence in flow systems, *Physica* **D33**, 1–20 (1988).
9. T. Bohr and O. B. Christensen, Size dependence, coherence, and scaling in turbulent coupled-map lattices, *Phys. Rev. Lett.* **63**(20), 2161–2164 (1989).
10. K. Kaneko, Spatiotemporal chaos in one- and two-dimensional coupled map lattices. *Physica* **D37**, 60–82 (1989).
11. K. Kaneko, Simulating physics with coupled map lattices, in *Formation, Dynamics and Statistics of Patterns*, edited by Kaneko K. *et al.* World Scientific, Singapore (1990).
12. H. Kook, F. N. Ling and G. Schmidt, Universal behaviour of coupled nonlinear systems, *Phys. Rev.* **A43**(6), 2700–2708 (1991).
13. M. J. Feigenbaum, Quantitative universality for a class of nonlinear transformations, *J. Stat. Phys.* **19**(1), 25–32 (1978).

14. M. J. Feigenbaum, The universal metric properties of nonlinear transformations, *J. Stat. Phys.* **21**(6), 669–706 (1979).
15. S. P. Kuznetsov, Universality and scaling in behaviour of coupled Feigenbaum systems, *Radiophys. Quant. Elect.* **28**(8), 681–695 (1985).

APPENDIX

We describe here the procedure allowing us to represent any weak coupling as a combination of the inertial and dissipative types.

It would be sufficient to consider the particular class of solutions. Let us define two sublattices, the first as a set of cells with the odd sum of indices $i + j$ and the second as a set with the even sum. Then we assume that the dynamical variable values coincide in all cells of each sublattice and are equal to u and v, respectively. Such solutions may be described by a system of two coupled maps

$$u_{l+1} = f(u_l) + \varepsilon\phi(u_l, v_l),\ v_{l+1} = f(v_l) + \varepsilon\phi(v_l, u_l), \tag{A.1}$$

where $\phi(u, v)$ is the coupling function vanishing for equal values of the arguments.

Let us consider long-period cycles of the map (A.1) in invariant subspace $u = v$ at the critical point $\lambda = \lambda_c$. Using the n-fold renormalization and rewriting the evolution operator (7) for the considered class of solutions we obtain

$$\begin{aligned} u &\to g(u) + \varepsilon[c_1 a^n \phi_1(u, v) + c_2 2^n \phi_2(u, v)], \\ v &\to g(v) + \varepsilon[c_1 a^n \phi_1(v, u) + c_2 2^n \phi_2(v, u)], \end{aligned} \tag{A.2}$$

where the proportionality of expansion factors to the coupling parameter ε is taken into account. Then the rescaled element of the period-2^n cycle is represented as the fixed point (u_*, u_*), where u_* is the root of the equation $u = g(u)$. We ask now: how do the multipliers of the cycles $\mu_n^{(1)*}$, $\mu_n^{(2)*}$ depend on n? Calculating the eigenvalues of the derivative matrix for the map (A.2) at the point (u_*, u_*) gives

$$\mu_n^{(1)} = g'(u_*),\ \mu_n^{(2)} = g'(u_*) + \varepsilon[c_1 D_1 a^n + c_2 D_2 2^n], \tag{A.3}$$

where $D_i = \frac{1}{2}[\partial\phi_i(u, v)/\partial u]_{u,v=u_*}$. Multipliers $\mu_n^{(1)}$ and $\mu_n^{(2)}$ concern symmetric and antisymmetric perturbations of the fixed point, respectively.

Thus, to analyze the 'composition' of coupling in a given system of coupled maps, it is necessary to find a sequence of (unstable) period-2^n cycles with $u = v$ at the point $\lambda = \lambda_c$ and to calculate the derivatives of their multipliers $\kappa_n = (\partial\mu_n^{(2)}/\partial\varepsilon)_{\varepsilon=0}$. They must obey the relation $\kappa_n = c_1 D_1 a^n + c_2 D_2 2^n$ and this fact allows us to find the coefficients of expansion.

Let us take, for example, the system with linear coupling

$$u_{l+1} = f(u_l) + \varepsilon(v_l - u_l),\ v_{l+1} = f(v_l) + \varepsilon(u_l - v_l). \tag{A.4}$$

Substituting $f(u) = 1 - \lambda u^2$, $\lambda = \lambda_c = 1.401155$ and performing the proposed calculations we present the results in Fig. 15 using coordinates $X = (a/2)^n$, $Y = \kappa_n 2^{-n}$. According to the consideration given above, the points lie on the straight line $Y = c_1 D_1 X + c_2 D_2$ and from the plot we find $c_1 D_1 = -1.821$ and $c_2 D_2 = -0.281$. So, in this case we have the combination of inertial and dissipative coupling.

For the system with quadratic coupling

$$u_{l+1} = f(u_l) + \varepsilon(f(v_l) - f(u_l)),\ v_{l+1} = f(v_l) + \varepsilon(f(u_l) - f(v_l)), \tag{A.5}$$

one finds $c_1 D_1 = 0$ and $c_2 D_2 = 3.202$ (see Fig. 15). This coupling is fully dissipative. Evidently, the combination of both coupling types in the proportion of 1:0.088 will give the pure inertial coupling.

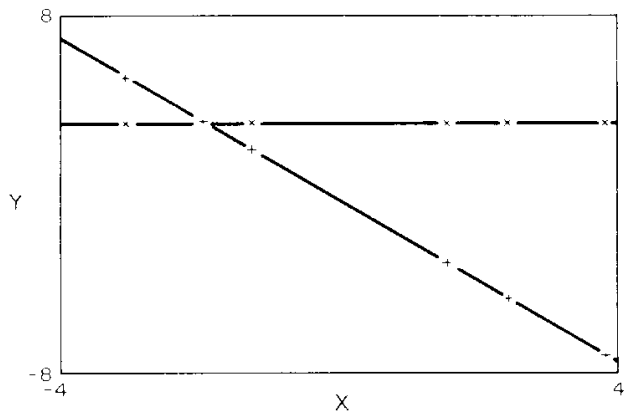

Fig. 15. Plot for calculation of the coupling composition in the map (A.1) with linear (+) and quadratic (×) coupling.